Int. J. Electrochem. Sci., 9 **(2014)** 5177 - 5186

International Journal of
ELECTROCHEMICAL
SCIENCE
www.electrochemsci.org

Development of Nickel Oxide and Manganese Oxide Nanostructured Binary Modified Anodes for Methanol Electro-Oxidation

Ghada H. El-Nowihy[1], *Ahmad M. Mohammad*[1,2,*], *Mostafa M.H. Khalil*[3], *Mohamed S. El-Deab*[1,2,*]

[1]Department of Chemical Engineering, Faculty of Engineering, The British University in Egypt, Cairo 11837, Egypt
[2]Chemistry Department, Faculty of Science, Cairo University, Cairo 12613, Egypt
[3]Chemistry Department, Faculty of Science, Ain Shams University, Cairo 11566, Egypt
[*]E-mail: ammohammad@cu.edu.eg; msaada68@yahoo.com

Received: 13 April 2014 / *Accepted:* 24 May 2014 / *Published:* 16 June 2014

In this investigation, a nanoparticle-based binary catalyst composed of nickel oxide (nano-NiO_x) and manganese oxide (nano-MnO_x), both were assembled on a platinum substrate, was developed for the direct methanol electro-oxidation (MO) in an alkaline medium. The morphological investigation was performed using field-emission SEM and revealed the electrodeposition of MnO_x in a nanorod structure and NiO_x in round-shaped nanospheres. The electrocatalytic activity of the modified electrodes towards MO depended critically on the order of deposition of the two oxides. The optimum electrocatalytic activity was obtained at the MnO_x/NiO_x/Pt electrode (in which nano-NiO_x was directly electrodeposited onto the Pt surface followed by nano-MnO_x) with a total surface coverage of ca. 86%. Both nano-NiO_x and nano-MnO_x are believed to act as catalytic mediators facilitating the adsorption of methanol and the charge transfer during MO.

Keywords: Fuel cells; Methanol electro-oxidation; Nickel oxide nanoparticles; Manganese oxide nanoparticles; Electrocatalysis.

1. INTRODUCTION

The global demand for renewable energy resources replacing the traditional fossil fuels and the urgency to sustain green societies have motivated intensively research on the development of fuel cells (FCs) [1,2]. For long time, the traditional hydrogen/oxygen fuel cells have attracted a global attention for their potential in providing energy and reducing the polluting emissions [3]. However, the risky environment surrounding the H_2 transportation and storage has motivated the replacement of H_2 fuel

with liquid fuels. Of these, methanol (in direct methanol fuel cells - DMFCs) and formic acid (in direct formic acid fuel cells - DFAFCs) appeared promising in terms of the ease handling and transporting. However, the DMFCs have a higher theoretical energy density (4690 Wh L^{-1}) if compared to DFAFCs (2086 Wh L^{-1}) [4].

In fact, the commercialization of DMFCs encountered two essential problems which ultimately induce a deterioration of their overall catalytic efficiency and durability [5]. The first is arising from the crossover of methanol through the Nafion membrane from the anodic to cathodic compartment of the fuel cell. Subsequently, methanol can continue the oxidation at the cathode simultaneously (Mixed Potential) with the oxygen reduction reaction (ORR). This, in turns, leads to a significant loss of the fuel, lowering the cathode potential, and decreasing the cell voltage [5]. Overcoming the crossover could successfully be tackled by functionalizing the Nafion membrane with groups resisting the methanol crossover. In this regard, the development of bilayer composite membrane composed of sulfonated graphene oxide (SGO)/Nafion and sulfonated activated carbon (SAC)/Nafion exhibited a low methanol crossover and a high proton conductivity [5,6]. Alternatively, the development of a cathodic catalyst selective for ORR but inactive for MO, as Ru-based Chalcogenides and oxides [5,7], could improve the overall cell performance.

The other major problem encountering the commercialization of DMFCs is related to the generation of several poisoning intermediates at the anode during the methanol electro-oxidation (MO) which induces a considerable reduction in the electrocatalytic activity of the anode. In this regard, the development of efficient electrocatalysts for the direct MO with high tolerance to poisoning intermediates is an issue of a prime importance.

So far, platinum, although expensive, represents a unique choice as an electrocatalyst for MO, as it provides a suitable base for the adsorption and dehydrogenation of methanol [8,9]. The poisoning of Pt with the reaction intermediates of MO has motivated the modification of Pt with several materials including the metallic and/or metal oxide alloys of Ru [8,10-16], Pb [17], MnO_x/Ru [18,19] in order to shift the reaction pathway of MO exclusively into CO_2 and H_2O (direct pathway).

Herein, we report on the development of a binary catalyst composed of nickel oxide (nano-NiO_x) and manganese oxide (nano-MnO_x) nanostructures which are electrochemically deposited onto Pt surface for the direct MO in alkaline medium. The influence of the order of deposition of the two oxides on the catalytic activity of the modified catalyst towards MO is addressed.

2. EXPERIMENTAL

2.1. Electrodes and pretreatments

A polycrystalline Pt (d = 1.6 mm) electrode served as a working electrode after cleaning by applying conventional procedures [20]. Typically, the electrode was mechanically polished with aqueous slurries of successively finer alumina powder (down to 0.06 μm) then washed thoroughly with distilled water. Then, the electrode was electrochemically pretreated by scanning the potential between the onset potentials of the H_2 and O_2 evolution reactions in 0.5 M H_2SO_4 for several cycles until a

characteristic cyclic voltammogram (CV) of a clean Pt surface was obtained. A platinum spiral wire and an Ag/AgCl/KCl (sat.) were employed as the counter and reference electrodes, respectively. All potentials in this investigation are recorded with respect to the reference electrode. Electrochemical measurements were conducted in a conventional two-compartment three-electrode glass cell using a Bio-Logic SAS potentiostat (model SP-150) operated with EC-Lab software. All chemicals used in this investigation were of analytical grade (Merck or Sigma Aldrich), and were used without further purification.

2.2. Electrode's modification

The modification of Pt electrodes with nano-NiO_x was achieved in two sequential steps. First, metallic Ni was deposited by a potentiostatic electrolysis in 0.1 M acetate buffer solution (ABS, pH = 4.0) containing 1 mM $Ni(NO_3)_2$ at −1.0 V for 3 min. Next, a passivation process of Ni is performed in 0.1 M phosphate buffer solution (PBS, pH = 7) by cycling the potential between −0.5 and 1 V for 10 cycles at a scan rate of 200 mV s^{-1} [21,22]. On the other hand, the modification with nano-MnO_x was achieved by cycling the potential from 0 to 0.4 V in 0.1 M Na_2SO_4 containing 0.1 M $Mn(CH_3COO)_2$ for 15 cycles at potential scan rate of 20 mV s^{-1}. The influence of the deposition order of the two oxides *i.e*, (nano-NiO_x and nano-MnO_x) was investigated by keeping the number of potential cycles involved in the deposition of nano-MnO_x constant at 15 cycles and the deposition time of nano-NiO_x was 3 min.

2.3. Materials Characterization

A field-emission scanning electron microscope (FE-SEM) (FEI, QUANTA FEG 250) was employed to evaluate the electrode's morphology. X-ray diffraction, XRD, (PANalytical, X'Pert PRO) operated with Cu target (λ = 1.54Å) was used to identify the crystallographic structure of nano-NiO_x and nano-MnO_x.

3. RESULTS AND DISCUSSION

3.1. Morphological and compositional analysis

Figure 1 depicts the SEM images of (A) $MnO_x/NiO_x/Pt$ and (B) $NiO_x/MnO_x/Pt$ electrodes. Interestingly, Fig. 1A shows that nano-MnO_x was intensively deposited onto the NiO_x/Pt electrode (most likely on the uncovered area of the Pt surface) in a network of nanorod arrays with an average diameter of *ca.* 15 nm. On the other hand, Fig. 1B displays the morphology of the $NiO_x/MnO_x/Pt$ electrode differently; where nano-NiO_x could effectively concealed the nanorod structure of nano-MnO_x (observed in Fig. 1A) and the surface appeared with round-shaped spheres of nano-NiO_x (average particle size was ca. 80 nm).

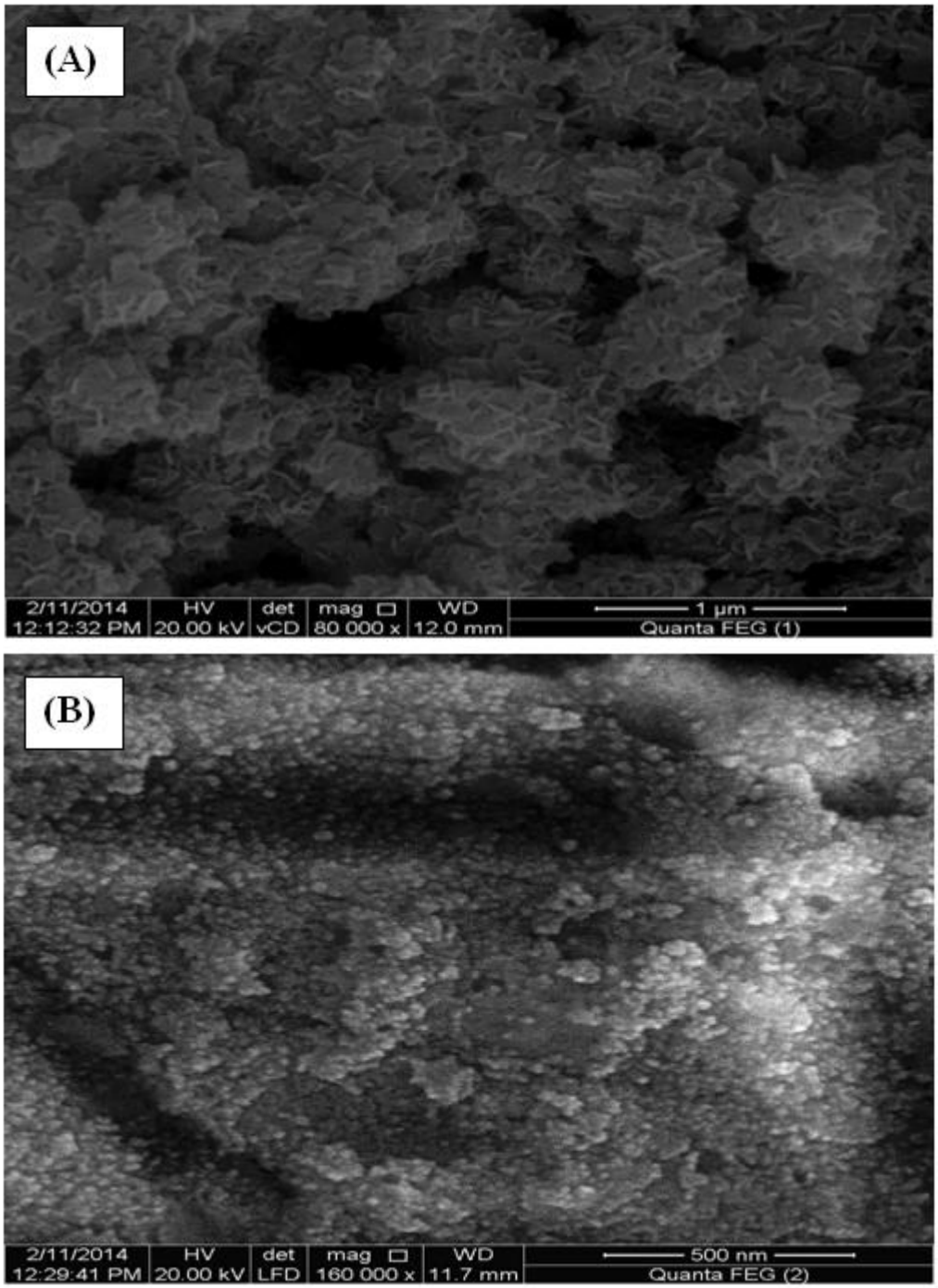

Figure 1. FE-SEM images for (A) $MnO_x/NiO_x/Pt$ and (B) $NiO_x/MnO_x/Pt$ electrodes. Nano-MnO_x and nano-NiO_x were electrodeposited onto the Pt surface as described in the experimental section.

XRD was next employed to disclose the phases of nano-NiO_x and nano-MnO_x deposited onto the Pt surface. Figure 2 showing XRD pattern of the $MnO_x/NiO_x/Pt$ electrode which revealed only the diffraction peaks corresponding to the different facets of poly-crystalline Pt substrate [23] at 2θ of ca. 39, 46, 67, 81, 86°. It was really difficult to observe the diffraction peaks of nano-NiO_x and nano-MnO_x using this spectroscope, presumably due to the low Ni and Mn contents in the detected depth (~ 10 µm) of XRD technique. However, this does not deny the existence of nano-MnO_x and nano-NiO_x

atop the Pt surface (*c.f.* Fig. 3). A similar observation was previously reported on polycrystalline Pt substrate [24]. However, under the same deposition conditions employed in this investigation, the β-NiOOH phase of nano-NiO_x on a glassy carbon (GC) substrate [24] could be identified. The γ-MnOOH phase of nano-MnO_x could also be identified, similarly, on Pt substrate but under critical and skillful handling [25].

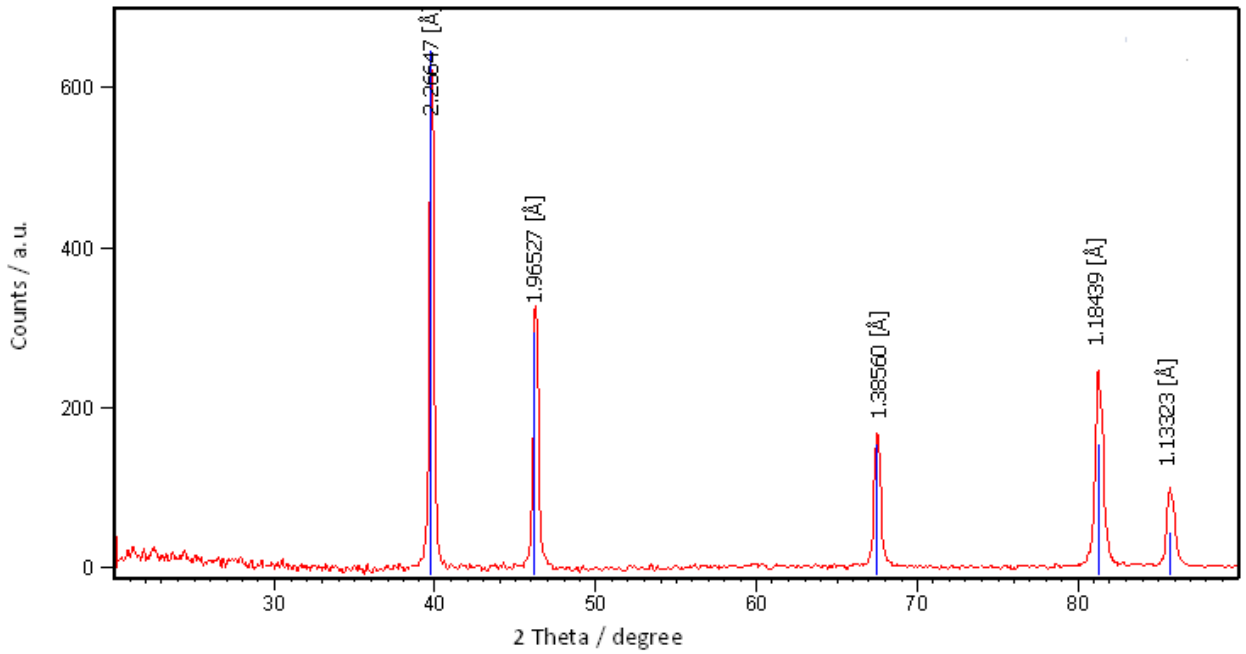

Figure 2. XRD pattern of MnO_x/NiO_x/Pt electrode. Scan speed 0.05°/s.

3.2. Electrochemical characterization

The electrochemical characterization is actually perfect in identifying the minor traces of electro-active species as those of Pt, Ni, and Mn. Figure 3 shows CVs measured in 0.1 NaOH at (a) unmodified Pt, (b) NiO_x/Pt, (c) NiO_x/MnO_x/Pt, and (d) MnO_x/NiO_x/Pt electrodes. The typical characteristic behavior of a polycrystalline Pt electrode in alkaline media is clearly shown in Fig. 3a; the oxidation of Pt, which extends over a wide range of potential, is coupled with the reduction peak at ca. –0.26 V. In addition, well-defined peaks for the H_2 adsorption/desorption ($H_{ads/des}$) are shown in the potential range from –0.6 to –0.9 V. However, at nano-NiO_x/Pt (Fig. 3b), a noticeable decrease in the intensity of the reduction peak of the Pt oxide is observed along with a decrease in the current of the $H_{ads/des}$ peaks. Another redox couple is observed, at ca. 0.4 V, which corresponds to the $Ni(OH)_2$/NiOOH transformation [26]. At the NiO_x/MnO_x/Pt (Fig. 3c) and MnO_x/NiO_x/Pt (Fig. 3d) electrodes, the reduction peak of Pt oxide and the $H_{ads/des}$ peak currents continued decreasing. However, the peak current of the Ni(II)/Ni(III) redox couple is markedly enhanced at NiO_x/MnO_x/Pt electrode (Fig. 3c, where nano-MnO_x is first deposited), compared to that at NiO_x/Pt electrode (curve b). This enhancement is consistent with the heavy deposition of nano-NiO_x revealed by SEM (Fig. 1B). It may also be attributed to the increase of the Ni(III) content by mixing nano-NiO_x with nano-

MnO_x. According to Das *et al*. [27,28], Mn (IV) can be converted during the anodic scan to Mn (V), which is a powerful oxidant and can further oxidize Ni(II) to Ni(III) resulting in an increase in the peak current.

$$Mn(V) + Ni(II) \rightarrow Ni(III) + Mn(IV) \quad (1)$$

At MnO_x/NiO_x/Pt electrode (Fig. 3d, where nano-NiO_x is first deposited onto Pt surface), the current of the Ni(II)/Ni(III) couple was significantly decreased in comparison to the NiO_x/Pt electrode, probably due to the partial deposition of nano-MnO_x on the previously deposited nano-NiO_x consistently with the SEM images shown in Fig. 1A.

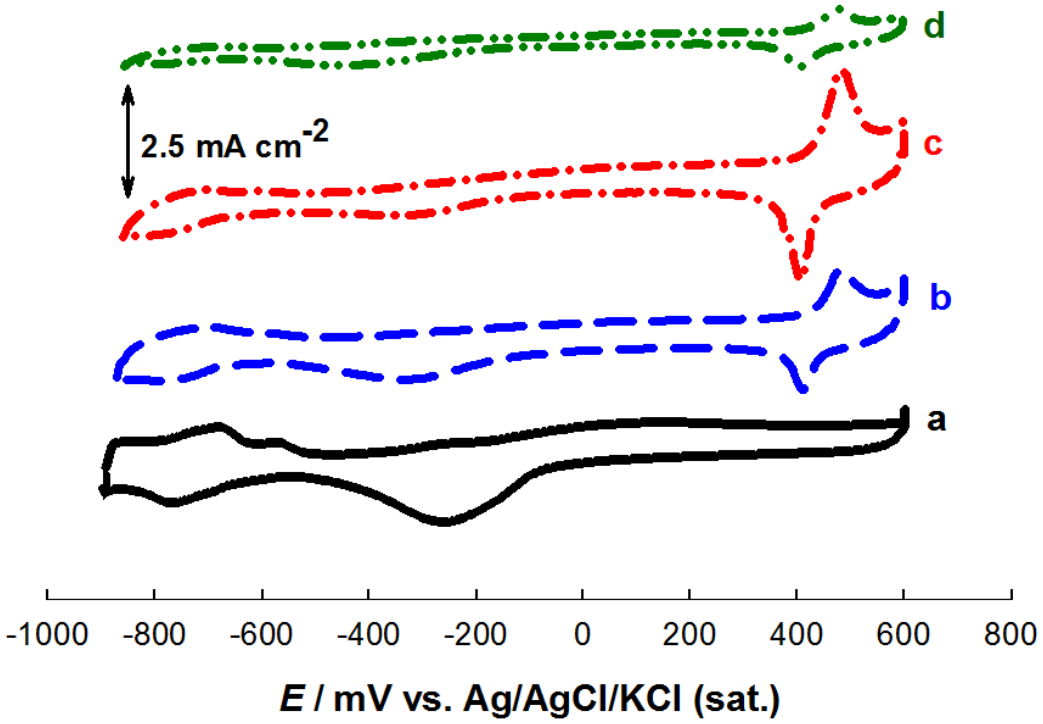

Figure 3. CVs measured in N_2-saturated 0.1 M NaOH at (a) bare Pt, (b) NiO_x/Pt, (c) NiO_x/MnO_x/Pt, and (d) MnO_x/NiO_x/Pt electrodes. Potential scan rate: 100 mV s^{-1}. N.B. Current densities were calculated on the basis of the geometric surface area of the Pt electrode.

3.3. Electrocatalytic oxidation of methanol

Figure 4 displays positive-potential going linear sweep voltammograms (LSVs) measured in NaOH solution containing 0.3 M methanol at (a) unmodified Pt, (b) NiO_x/Pt, (c) NiO_x/MnO_x/Pt, and (d) MnO_x/NiO_x/Pt electrodes. As clearly shown in Fig. 4a, the smallest oxidation current (at ca. −150 mV) was observed for MO at the bare (i.e., unmodified) Pt electrode. This is likely because the poisoning effect with several intermediates such as ($-CH_2OH$, $=CHOH$, $\equiv COH$, CO and HCOOH), which consume an appreciated part of the Pt surface, deteriorating its catalytic activity. However, at the NiO_x/Pt electrode (Fig. 4b), the MO current increases, concurrently, with a negative shift in the

onset potential of MO. This, definitely, accounts for a significant enhancement (catalysis) in MO, which may be induced from the Ni(II)/Ni(III) transformation that is believed to facilitate the charge transfer of MO according to the following equations; [29,30]

$$\text{Ni(III)} + \text{methanol} \rightarrow \text{intermediate} + \text{Ni(II)} \quad (2)$$

$$\text{Ni(III)} + \text{intermediate} \rightarrow \text{products} + \text{Ni(II)} \quad (3)$$

The peak current of MO continued increasing after the binary modification of the Pt electrode with nano-NiO_x and nano-MnO_x and the onset potential of MO was shifted towards the cathodic direction (see Table 1). However, the degree of enhancement in the catalytic activity exhibited at the MnO_x/NiO_x/Pt electrode (Fig. 4d) was higher than that observed at the NiO_x/MnO_x/Pt electrode (Fig. 4c). This signifies the importance of being nano-MnO_x exposed to the surface in the vicinity of the electrolyte. We wish here to emphasize that the deposition of nano-NiO_x onto the MnO_x/Pt electrode was intensive to conceal the nanowire structure of nano-MnO_x (as revealed from Fig. 1B).

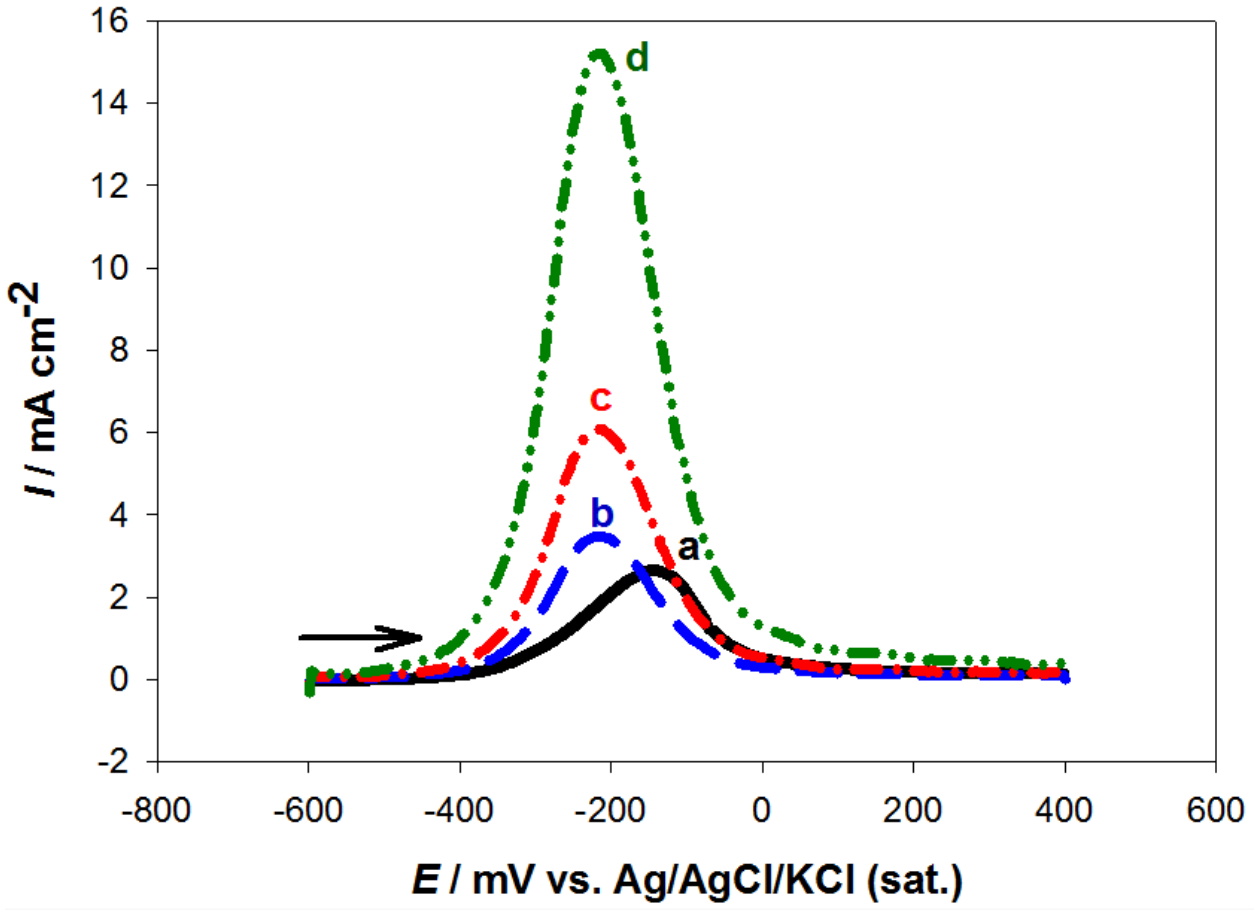

Figure 4. LSVs for MO at (a) bare Pt, (b) NiO_x/Pt, (c) NiO_x/MnO_x/Pt, and (d) MnO_x/NiO_x/Pt electrodes in N_2-saturated 0.1 M NaOH solutions containing 0.3 M methanol. Potential scan rate is 50 mV s^{-1}. N.B. Current densities were calculated on the basis of the real surface area of the bare and modified Pt electrodes.

On the other hand, the deposition of nano-MnO_x onto the NiO_x/Pt electrode resulted in the direct exposure of nano-MnO_x (Fig. 1A) and nano-NiO_x (see the Ni(II)/Ni(III) transformation peaks in Fig. 3d) to the electrolyte. Hence, we believe that the influence of both of nano-MnO_x and nano-NiO_x in the MnO_x/NiO_x/Pt electrode (Fig. 4d) is much greater than that at the NiO_x/MnO_x/Pt electrode (Fig. 4c). It remains to understand the role of nano-MnO_x in reinforcing the catalytic activity of the NiO_x/Pt electrode towards MO. The following points may assist in this regard:

1- Nano-MnO_x may play a role in retrieving the nano-NiO_x from poisoning intermediates to leave the nano-NiO_x active sites available for methanol adsorption [27,31],

2- Nano-MnO_x may increase the Ni(III) content of nano-NiO_x according to Eq. 1; which consequently enhances the electron conduction of the matrix and MO as well [27,28],

3- The facilitated adsorption of methanol onto nano-MnO_x via hydrogen bonding may account on this enhancement [27,28],

4- The reversible transformation of MnOOH/MnO_2 produces MnO_2, which is a powerful oxidant and is thought to provide oxygen to adjacent intermediates as CO to facilitate its oxidation into CO_2, retrieving the Pt surface for MO [32,33,34,35]:

$$2MnOOH + 2OH^- \leftrightarrow 2MnO_2 + 2H_2O + 2e^- \quad (4)$$

$$2MnO_2 + Pt - CO_{ads} + H_2O \rightarrow 2MnOOH + Pt_{free} + CO_2 \quad (5)$$

Addition of Eqs. 4 and 5 gives:

$$Pt - CO_{ads} + 2OH^- \rightarrow Pt -_{free} + CO_2 + H_2O + 2e^- \quad (6)$$

5- Finally, the lower catalytic enhancement of MO at the NiO_x/MnO_x/Pt electrode may be affected by changing the active phase of nano-MnO_x (γ-MnOOH) during the passivation step converting metallic nickel into nano-NiO_x.

Table 1. Variation of the catalytic enhancement factor and the onset potential for MO at various Pt modified electrodes in 0.1 M NaOH + 0.3 M methanol.

Electrode	Surface Coverage[a] / θ,%	E_{onset}[b] / V	Enhancement factor[c]	I_p / mA cm^{-2}
Unmodified Pt	-----	−0.35	-----	2.6
Nano-NiO_x/Pt	66	−0.41	1.3	3.5
Nano-NiO_x/nano-MnO_x/Pt	85	−0.45	2.3	6.0
Nano-MnO_x/nano-NiO_x/Pt	86	−0.52	5.8	15.2

[a] The values of surface coverage (θ) were calculated for the various modified Pt electrodes where ($\theta = 1 - S_{modified}/S_{unmodified}$). $S_{modified}$ and $S_{unmodified}$ refer to the real surface area of the modified and the

unmodified Pt electrodes, respectively, obtained from the amount of charge associated with the reduction of PtO at ca. – 0.26 V (see Fig. 3) using a reported value of 420 μC cm^{-2} [36].

[b] The values of the onset potential of MO were measured at a constant current density of 200 μA cm^{-2} for all electrodes.

[c] The enhancement factor for MO was calculated by dividing I_p of MO at the modified Pt electrode by I_p of MO at the bare one.

In general, we believe that both of nickel oxide (nano-$NiO_{x)}$ and manganese oxide (nano-$MnO_{x)}$ nanostructures could effectively act as catalytic mediators in such a way that facilitating the charge transfer involved in MO.

4. CONCLUSION

We have successfully developed a binary catalyst for methanol electro-oxidation (MO) in alkaline medium. The fabrication of the catalyst involved the electrodeposition of nickel oxide (nano-NiO_x) and manganese oxide (nano-MnO_x) nanostructures onto a Pt substrate. The order of deposition of the two oxides affected the catalytic activity towards MO. The highest catalytic enhancement for MO was achieved at MnO_x/NiO_x/Pt electrode, where nano-NiO_x was first deposited onto the Pt surface followed by nano-MnO_x. The peak current of MO at this electrode was almost five times larger than that obtained at the unmodified Pt. Nano-NiO_x (in β-NiOOH phase) and nano-MnO_x (in γ-MnOOH phase) are believed to mediate the oxidation scheme of MO in such a way facilitating the charge transfer and/or remove the poisoning intermediates.

References

1. J. M. Feliu and E. Herrero, in: W. Vielstich, H. A. Gasteiger and A. Lamm (Eds.), *Handbook of Fuel Cells*, Vol. 2, Wiley, New York (2003).
2. (a) A. M. Abdullah, T. Okajima, A.M. Mohammad, F. Kitamura, T. Ohsaka, *J. Power Sources*, 172 (2007) 209–214; (b) A. M. Abdullah, A.M. Mohammad, T. Okajima, F. Kitamura, T. Ohsaka, *J. Power Sources*, 190 (2009) 264–270.
3. D. -H. Lee , C. P. Hungb, *Int. J. Hydrogen Energy,37 (2012)* pp. 15753–15754
4. Y. Zhu, S. Y. Ha, R. I. Masel, *J. Power Sources*, 130 (2004) pp. 8–14
5. M. Hogarth, G. Hoogers, E. Chen, D. Thompsett, R. Stone, D. Hart, Prospects of the Direct Methanol Fuel Cell, in *Fuel cell Technology Handbook*, Gregor Hoogers (Ed.) , chapter 7, pp. 4-11, CRC Press LLC (2003).
6. L. D. Tsai, H. C. Chien, W. H. Huang, C. P. Huang, C. y. Kang, J. N. Lin, and F. C. Chang, *Int. J. Electrochem. Sci.*, 8 (2013)
7. M. Montiel, P. Hernández-Fernández, J.L.G. Fierro, S. Rojas, P. Ocón, *Journal of Power Sources*, 191(2009), pp. 280-288
8. A. A. Al-Shafei, R. Hoyer, L. A. Kibler and D. M. Kolb, *J. Electrochem. Soc*., 151 (2004) F141.
9. N. S.-Alvarez, L. R. Alden, E. Rus, H. Wang, F. J. DiSalvo and H. D. Abruna, *J. Electroanal. Chem.*, 626 (2009) 14.
10. J. O'M. Bockris and H. Wroblowa, *J. Electroanal. Chem.*, 7 (1964) 428.

11. H. Binder, A. Kohling and G. Sanstede, *From Electrocatalysis to Fuel Cells*, G. Sanstede (Ed.), University of Washington, Seattle, (1972).
12. H. A. Gasteiger, N. M. Markovic, P. N. Ross and E. J. Cairns, *J. Phys. Chem.*, 98 (1994) 617.
13. H. Nonaka and Y. Matsumura, *J. Electroanal. Chem.*, 520 (2002) 101.
14. S. Lj. Gojkovic, T. R. Vidakovic and D. R. Durovic, *Electrochim. Acta*, 48 (2003) 3607.
15. Z. Jusys, J. Kaiser and R. J. Behm, *Electrochim. Acta*, 47 (2002) 3693.
16. A. O. Neto, R. W. R. V.-Silva, M. Linardi and E. V. Spinacé, *Int. J. Electrochem. Sci*., 4 (2009) 954.
17. B. Beden, F. Kadirgan, C. Lamy and J. M. Leger, *J. Electroanal. Chem.*, 127 (1981) 75
18. J. S. Rebello, P. V. Samant, J. L. Figueiredo and J. B. Fernandes, *J. Power Sources*, 153 (2006) 36.
19. G.-Y. Zhao and H.-L. Li, *Appl. Surf. Sci.*, 254 (2008) 3232.
20. G. M. Swain, Solid Electrode Materials: Pretreatment and Activation, in, *Handbook of Electrochemistry*, Cynthia G. Zoski (Ed.) , chapter 5, p 145, Elsevier, UK (2007)
21. D. Giovanelli, N.S. Lawrence, L. Jiang, T.G.J. Jones, R.G. Compton, *Sensors and Actuators B: Chemical*, 88 (2003) 320.
22. D. Giovanelli, N.S. Lawrence, S.J. Wilkins, L. Jiang, T.G.J. Jones, R.G. Compton, *Talanta*, 61 (2003) 211.
23. T. Hyde, *Platinum Metals Rev.*, 2008, 52, (2), pp. 129–130
24. G. A. El-Nagar, A. M. Mohammad, M. S. El-Deab and B. E. El-Anadouli, *J. Electrochem. Soc.*,159 (2012) 250
25. M. S. El-Deab, *Int. J. Electrochem. Sci.*, 4 (2009) 1332
26. A. Fundo and L. Abrantes, *J. Electroanal. Chem.*, 600 (2007) 63.
27. D. Das, P.K. Sen, K. Das, *Electrochim. Acta*, 54 (2008) 289.
28. D. Das, P.K. Sen, K. Das, *J. Electroanal. Chem.*, 611 (2007) 19.
29. J. Taraszewska, G. Rosłonek, *J. Electroanal. Chem.*, 364 (1994) 209.
30. J.R. Allen, A. Florido, S.D. Young, S. Daunert, L.G. Bachas, *Electroanalysis*, 7 (1995) 710.
31. I.-H. Yeo, D.C.Johnson, *J. Electroanal. Chem.*, 484 (2000) 157.
32. M. S. El-Deab and T. Ohsaka, *J. Electrochem. Soc.*, 155 (2008) D14
33. M. Pourbaix, in *Atlas of Electrochemical Equilibria in Aqeous Solutions*, Pergamon Press, Oxford, (1966) p. 286.
34. S. Fierro, T. Nagel, H. Baltruschat and C. Comminellis, *Electrochem. Commun.*, 9 (2007) 1969.
35. S. Ardizzone and S. Trasatti, *Adv. Colloid Interface Sci.*, 64 (1996) 173.
36. S. Trasatti and O. A. Petrii, *Pure & Appl. Chem*., 63 (1991) 711.